Atmos. Chem. Phys. Discuss., 14, 3193–3230, 2014
www.atmos-chem-phys-discuss.net/14/3193/2014/
doi:10.5194/acpd-14-3193-2014

Atmospheric Chemistry and Physics Discussions

Analysis of the global atmospheric methane budget using ECHAM-MOZ simulations for present-day, pre-industrial time and the Last Glacial Maximum

A. Basu[1,*], M. G. Schultz[1], S. Schröder[1], L. Francois[2], X. Zhang[3], G. Lohmann[3], and T. Laepple[3]

[1]IEK-8, Forschungszentrum Jülich, Wilhelm-Johnen-Str., 52425 Jülich, Germany
[2]Unité de Modélisation du Climat et des Cycles Biogéochimiques, University of Liège, Liege, Belgium
[3]Alfred Wegener Institute for Polar and Marine Research, Bremerhaven, Germany
[*]now at: Institute of Marine and Atmospheric Research Utrecht, Utrecht University, the Netherlands

Received: 15 November 2013 – Accepted: 9 January 2014 – Published: 31 January 2014

Correspondence to: A. Basu (a.basu@uu.nl)

Published by Copernicus Publications on behalf of the European Geosciences Union.

Abstract

Atmospheric methane concentrations increased considerably from pre-industrial (PI) to present times largely due to anthropogenic emissions. However, firn and ice core records also document a notable rise of methane levels between the Last Glacial Maximum (LGM) and the pre-industrial era, the exact cause of which is not entirely clear. This study investigates these changes by analyzing the methane sources and sinks at each of these climatic periods. Wetlands are the largest natural source of methane and play a key role in determining methane budget changes in particular in the absence of anthropogenic sources. Here, a simple wetland parameterization suitable for coarse-scale climate simulations over long periods is introduced, which is derived from a high-resolution map of surface slopes together with various soil hydrology parameters from the CARAIB vegetation model. This parameterization was implemented in the chemistry general circulation model ECHAM5-MOZ and multi-year time slices were run for LGM, PI and present-day (PD) climate conditions. Global wetland emissions from our parameterization are 72 $Tg\,yr^{-1}$ (LGM), 115 $Tg\,yr^{-1}$ (PI), and 132 $Tg\,yr^{-1}$ (PD). These estimates are lower than most previous studies, and we find a stronger increase of methane emissions between LGM and PI. Taking into account recent findings that suggest more stable OH concentrations than assumed in previous studies, the observed methane distributions are nevertheless well reproduced under the different climates. Hence, this is one of the first studies where a consistent model approach has been successfully applied for simulating methane concentrations over a wide range of climate conditions.

1 Introduction

Methane (CH_4) is one of the most abundant organic trace gases in the atmosphere. It is emitted both from anthropogenic and biogenic sources across the globe and its main loss process is reaction with the hydroxyl radical (OH) in the atmosphere. Its strong

ACPD
14, 3193–3230, 2014

global warming potential (30 times more than CO_2 per molecule), along with its role in regulating atmospheric chemistry makes it a key player in the earth–atmosphere feedback. When combining the in-situ measurements from the global network established over the past few decades (Dlugokencky et al., 1998; Cunnold et al., 2002; Morimoto et al., 2006), with ice core analysis dating back up to 650 kyr before present (Chappellaz et al., 1990, 1997; Blunier et al., 1995; Etheridge et al., 1998; Spahni et al., 2005) one can obtain a relatively clear picture of the global methane concentration changes from prehistoric periods to the present. Methane records preserved in gas bubbles both at Greenland and Antarctica ice cores reveal that from Last Glacial Maximum (LGM ~ 21 kyr before present) to pre-industrial era (PI ~ 200 yr before present), methane concentrations rose from 360 ppb up to 700 ppb (Chappellaz et al., 1997; Stauffer et al., 1988). With the advent of global industrialization a gradual increase in global methane concentration is observed till the late 1990s when it reaches 1750 nmol mol^{-1}.

Several numerical model studies have investigated the contributions of the different sources and sinks to the global methane budget during LGM, PI, or PD conditions. Some studies investigated the changes between LGM and PI (Levine et al., 2011; Kaplan et al., 2006; Valdes et al., 2005; Weber et al., 2010; Dällenbach et al., 2000), or between PI and PD (Wuebbles et al., 2002; Houweling et al., 2000b; Dlugokencky et al., 1994, 1995, 1998; Khalil and Ramussen, 1987), but none addressed the changes between all three periods with a single, consistent model set-up. Among the existing model studies, notable uncertainties remain pertinent in estimating total source strength of methane emissions and attributing the cause to changes in global methane budget. The PD methane sink due to the reaction with OH appears relatively well constrained (±20 %), because of recent advances in the interpretation of methylchloroform records (Montzka et al., 2011). With respect to the PI and LGM methane budgets, estimates of the emissions from wetlands as the dominating natural source diverge, and different assumptions have been made concerning the changes of the atmospheric OH concentration (Cao et al., 1996; Valdes et al., 2005; Webber et al., 2010).

ACPD
14, 3193–3230, 2014

In this study, we present a new wetland methane emission parameterization, which is suitable for use in global coarse resolution chemistry climate simulations. The wetland scheme was implemented in the ECHAM-MOZ chemistry general circulation model and was used for a consistent set of simulations for LGM, PI, and PD climate conditions. A particular strength of our parameterization is its ability to capture the regional distribution of wetlands relatively well, owing to the fine spatial resolution of 10 min for the orography and hydrological data that were used as input. The ECHAM-MOZ simulation results are evaluated with available station observation data and ice core records.

The manuscript is structured as follows: Sect. 2 describes the wetland parameterization and the simulation set-up of the ECHAM5-MOZ model. Section 3 discusses the choices made for methane emissions and sinks, respectively. In Sect. 4 we present and discuss results from the PD, PI, and LGM methane simulations. Section 5 discusses the changes of methane sources and sinks among the three climatic periods, and Sect. 6 contains the conclusions from this study.

2 Methods and model description

2.1 Wetland methane modeling

The wetland methane source parameterization consists of two steps. First the global potential wetlands are parameterized using CARAIB derived soil water content and terrain slopes. The strength of methane emission is then estimated from the potential wetlands following the empirical formula of Gedney et al. (2004) who used soil temperature and soil carbon as the control parameters.

The method of wetland parameterization is introduced in the study as a further step from the already existing similar method by Kaplan (2002), which is done at a coarser grid resolution of 0.5° to a much finer scale of 10 min for present day. It increases the possibility to capture wetland formation at sub-grid scale. Thus we try to adapt an

ACPD
14, 3193–3230, 2014

improved method not only to represent global wetland areas better but the regional wetlands as well. Apart from this, given the markedly different characteristics of boreal and tropical wetlands, a separate treatment for them is adapted in the parameterization method, which is discussed later in this section.

The CARAIB model (Warnant et al., 1994; Gérard et al., 1999; Otto et al., 2002; Laurent et al., 2008; Dury et al., 2011) is a large-scale vegetation model designed to study role of vegetation in the global carbon cycle. It contains a hydrological module which calculates soil water content and has a detailed parameterization of the hydrological fluxes in the root zone where methane production occurs. Soil water in CARAIB is computed relative to field capacity. For determination of potential wetland areas, threshold values for soil water content and terrain slope are selected to identify the areas which are sufficiently flat and moist. This approach is similar to Kaplan (2002), but differs in applying two different threshold values for normalized soil water content in latitudes north of 30° N and for the rest of the globe, only above which wetland formation is possible. However, the threshold value for surface slope is 2° everywhere, which is considered upper limit for wetland occurrences. The choice of two different thresholds for soil water content takes into account the different processes leading to wetland formation in northern boreal and mid latitudes and in the tropics, respectively. In the high northern latitudes, the wetland formation depends on the melting and thawing of accumulated snow, whereas in the tropics it is governed by the rainfall pattern.

Following Gedney et al. (2004), the methane emission rate from wetlands is considered linearly dependent on soil carbon and exponentially on soil temperature and expressed by the following equation.

$$\mathrm{CH_4\ emission} = K_{\mathrm{CH_4}} \cdot \mathrm{C_{soil}} \cdot Q_{10}^{(T_{\mathrm{soil}} - T_{\mathrm{ref}})/10}$$

In this relationship $K_{\mathrm{CH_4}}$ is a global constant, which is optimised in view of global methane flux. $\mathrm{C_{soil}}$ is the amount of decomposable carbon which works as a substrate for methanogenesis and Q_{10} is defined as a factor that determines the rate of reaction with 10 °C rise in temperature. Instead of one globally uniform scaling factor $K_{\mathrm{CH_4}}$ as

ACPD
14, 3193–3230, 2014

in the original publication, we optimized the global methane emission flux separately for regions north and south of 45° N, respectively. The K_{CH_4} value for boreal wetlands is about 80 % of the K value for other regions. The optimization was performed by comparing the seasonal distribution of present-day model results with data from the Global Atmosphere Watch World Data Center for Greenhouse Gases (WDCGG) (see Sect. 4.2). The resulting present-day annual global wetland emission source strength is 132 Tg, which is found to be in the low end of the estimates provided in IPCC (2007).

2.2 ECHAM5 MOZ climate model

The model used in the present study is the general circulation model ECHAM5 (Roeckner et al., 2003), which was extended to include the emissions, chemical transformations and sinks relevant to atmospheric methane.

The dynamical core of ECHAM5 solves the prognostic equations for vorticity, divergence, temperature, and the logarithm of surface pressure in spectral space with a pre-defined triangular cutoff at wave number 31, 42, 63, 106, etc. (spectral resolution). Physical processes such as advection of tracers and water vapor, convective and stratiform clouds, vertical diffusion, radiation and chemistry are calculated on an associated gaussian grid. The vertical axis uses a hybrid terrain-following sigma-pressure coordinate system (Simmons and Burridge, 1981). The model uses a semi-implicit leapfrog time integration scheme (cf. Robert, 1982) with a special time filter (Asselin, 1972). Details of the physical parameterizations including radiation, surface processes, gravity wave drag, convection, stratiform cloud formation, orbit variations, and subgrid scale orography can be found in Roeckner et al. (2003). In this study, the model was run in T42L31 resolution. This corresponds to a Gaussian grid with 128 longitudes and 64 latitudes (~ 2.8° × 2.8° resolution) and a vertical grid with 31 levels from the surface to 10 hPa.

The methane module consists of a simple chemistry parameterization using the ACCENT multi-model average climatology of monthly mean OH concentrations (M. Krol, personal communication, 2006; ACCENT is described by Stevenson et al., 2006), and

ACPD
14, 3193–3230, 2014

the rate coefficient k_{OH} of the $OH + CH_4$ reaction from the JPL 2011 report (Sander et al., 2011). Except for wetlands, methane emissions are prescribed as monthly mean fields (see Sect. 3). In addition to the main CH_4 sink due to reaction with OH, we also included a linear loss rate due to dry deposition, applying a globally constant value of $v = 8.5 \times 10^{-7}\,m\,s^{-1}$ for the deposition velocity over land surfaces (0 over the ocean). This results in a global methane loss rate due to dry deposition of $25\,Tg\,yr^{-1}$, for present day and PI.

For the present-day and pre-industrial simulations, sea surface temperatures (SST) and sea ice (SIC) fields were constrained by gridded fields from the Atmospheric Model Intercomparison Project 2 (AMIP2, Gates et al., 1999). For the LGM simulation, SST and SIC fields as well as all the other data including surface variables (surface geopotential, snow depth, surface roughness, orography) and initial conditions for temperature, divergence, specific humidity and vorticity are obtained from 50 yr output of coupled atmosphere-ocean-land simulations (Zhang et al., 2013) using the comprehensive Earth system model COSMOS (ECHAM5-JSBACH-MPIOM). This model was already utilized to analyse the last millennium (Jungclaus et al., 2010), warm Cenozoic climates (Knorr et al., 2011; Stepanek and Lohmann, 2012; Dowset et al., 2013), glacial (Kageyama et al., 2013; Gong et al., 2013; Zhang et al., 2013) and interglacial climates (Varma et al., 2012; Wei et al., 2012; Wei and Lohmann, 2012). Details of the glacial model set up and forcings are reported in Zhang et al. (2013). The 50 yr are taken from a quasi-steady state after 3000 yr of model integration. Obliquity, eccentricity and perihelion are set at values of 22.95°, 0.018994° and 294.42° respectively, and the LGM CO_2 concentration is fixed at $185\,\mu mol\,mol^{-1}$. In our set up of ECHAM MOZ, the initial methane mixing ratios are taken from Coupled Model Inter-comparison Project (CMIP5) paleoclimate simulations for LGM (Sueyoshi et al., 2013).

ACPD
14, 3193–3230, 2014

3 Methane sources and sinks

3.1 Emission inventories (other than wetlands) for present day

For the PD simulation, methane emissions from a variety of sources are used (Table 1). Emissions from anthropogenic sources are from EDGAR 3.2 (http://edgar.jrc.ec.europa.eu/index.php; P. Bergamaschi, personal communication, 2009). The seasonality of rice paddy emissions has been adapted from monthly data of Matthews et al. (1991). Biomass burning emissions are from the "Reanalysis of the tropospheric composition over the past 40 years" (RETRO) project (Schultz et al., 2008). This inventory was constructed using a combination of reported and simulated data on burned area in different world regions. The seasonality and geographic distribution of the fires was taken from a satellite burned area product (GBA-2000, Tansey et al., 2004). The biomass burning emissions were scaled by factor of 0.56 north of 35° N and by a factor of 1.48 south of 35° N in order to improve the seasonal cycle of present-day methane concentrations in comparison to the WDCGG data. The optimized biomass burning budget estimates 35 $\mathrm{Tg\,yr^{-1}}$. The global annual total of the anthropogenic sources including biomass burning amounts to 335 Tg (Table 1), which is well in the range of 307 to 428 Tg of other studies reported in IPCC (2007). We did not include a source either from geological seepage (Etiope, 2009) or from hydrates in any of our simulations. These two together could possibly contribute another 4–8 $\mathrm{Tg\,yr^{-1}}$ to our emissions. Although Etiope speculated about 3 Tg annual methane emission from Europe alone, further validation is needed.

3.2 Emission inventories for LGM and PI

There are considerable uncertainties in the methane source strengths both for PI and LGM. While it is clear that anthropogenic sources during these times were much lower than at present, there is some discussion in the literature (i.e. Ruddiman et al., 2001) about an already significant anthropogenic contribution during PI. Previous modeling

ACPD
14, 3193–3230, 2014

studies either included such contributions (Houweling et al., 2000a) or not (Valdes et al., 2005). There is evidence of domesticated animals as early as 10 000 yr ago (Gupta et al., 2004) and of rice agriculture starting by 7500 yr BP (Chang, 1976; Glover and Higham, 1996). In our PI simulation, we included the emissions from rice, livestock and animal waste as given by Ruddiman et al. (2001). Emission from wild animals is taken from Chappellaz et al. (1993) who estimated it from animal counts which is supported by Subak (1994). The strengths of ocean and biomass burning emissions are adopted from Valdes et al. (2005). As shown in Table 1, Valdes et al. (2005) estimated PI biomass burning emissions of 10 $Tg\,yr^{-1}$ which is lower than the estimate of Subak (1994) and less than a third of our present-day estimate. In the absence of other evidence, methane emissions from termites are retained at their present-day value.

The LGM simulations use the emission source strengths from Valdes et al. (2005) in all sectors except for wetlands where we apply our own parameterization, based on the soil moisture output from a LGM CARAIB simulation (Henrot et al., 2009). We note that this adds 8 $Tg\,yr^{-1}$ to the termite emissions (compared to PD and PI), while it reduces the emissions from the ocean and from biomass burning by the same amount. The LGM wetland source strength is discussed in Sect. 4.3.

3.3 Present-day methane sinks

As described above the atmospheric methane sink due to oxidation by OH was parameterized using a gridded monthly mean OH distribution from the multi-model mean of the ACCENT inter-comparison activity (M. Krol, personal communication, 2006). The annual tropospheric global mean OH concentration in this data set is 10.8×10^5 molecules cm^{-3}. This is close to the global OH estimates using methyl chloroform (Prinn et al., 2001; Krol et al., 2003) and ^{14}CO (Quay et al., 2000), which ranges between $9.4 \pm 1.3 \times 10^5$ and $10.7 \pm 0.17 \times 10^5$ molecules cm^{-3}, and model estimation (Shindell et al., 2001) which finds an average OH concentration of 9.76×10^5 molecules cm^{-3}. In the ACCENT project, 19 global models simulated the atmospheric composition around the year 2000 using different meteorological boundary conditions and different

ACPD
14, 3193–3230, 2014

emission inventories. The mean methane lifetime from these models is 8.67 yr (Stevenson et al., 2006), compared to the value of 8.4 yr from IPCC (2001).

3.4 PI and LGM methane sinks

There have been a series of atmospheric chemistry modeling studies which assessed changes in the tropospheric OH distribution in past climates compared to present day (Martinerie et al., 1995; Kaplan et al., 2006; Adams et al., 2001). The emission rate and atmospheric abundance of CO, CH_4, O_3, NO_x and other VOCs influence the OH concentration in the atmosphere. Most of the studies have found a post-industrial increase in OH due to large anthropogenic emission of NO. However disagreements are found among the modeling studies as the magnitude of changes in PI OH varies from −5 % to +20 % (Martinerie et al., 1995; Crutzen and Brühl, 1993; Thompson et al., 1993; Wang and Jacob, 1998; Lelieveld et al., 2008) compared to present day. In the recent multi model comparison ACCMIP study by Naik et al. (2013) on OH changes from PI to present day, it is found that the average OH concentration remains constant over this period (−0.6 ± 8.8 %), even though a large inter model diversity remains, particularly with respect to regional OH changes. This finding is strongly supported by Montzka et al. (2011) which endorses much lower variation in CH_3CCl_3, a proxy used in OH estimation, between PI and PD unlike the previous studies. However, according to Naik et al. (2013), the post-industrial increase in BVOCs contributed to OH loss (3.1 ± 3 %). Recent atmospheric chemistry studies (Hofzumahaus et al., 2009; Peeters and Mueller, 2010; Taraborrelli et al., 2012) have shown that BVOCs (in particular isoprene) exert much less control on OH concentrations than previously thought, although the exact chemical pathway of the apparent additional OH recycling is not entirely clear yet. In a scenario, with no feedback between BVOC and OH, the PI OH concentration could be lower than present day by at most 6.1 % following Naik et al. (2013). So at the present study, we consider two sets of PI methane simulations, one with present day OH and the other with OH reduced by 6 %.

ACPD
14, 3193–3230, 2014

Most of the chemistry studies estimated an increase in LGM OH between 18 and 25 % compared to PI. The high LGM OH concentration is assumed to result from low BVOC emissions which resulted from reductions in global forest cover and a cooler climate. However, other factors such as enhanced albedo, reduced water vapour and reduced NO_x emission from soil and lightning must also have influenced the LGM OH concentrations. To our knowledge no study has systematically looked at these factors yet. To include all these factors and to quantify their individual impacts on LGM OH changes compared to PI, a set of sensitivity experiments with the MOZART2 chemistry transport model (Horowitz et al., 2003) had been carried out (T. Laepple, personal communication, 2009). Figure 1 provides an overview about the possible PI-LGM OH changes derived from this experiment. It is evident from the figure that both reduced BVOC emission and methane flux during LGM affects in 26 % OH increment. Enhanced albedo and biomass burning also increase OH abundance. Together they contribute to OH enhancement by 60 %. However a reduced NO_x emission and atmospheric vapour content has an opposite effect and together reduces OH by 34 %. Overall, we estimate a net increase in LGM OH by 26 % compared to PI considering these counter effects. This chemistry study also includes the effect of the reduced reaction rate of the $OH+CH_4$ reaction due to lower temperatures during the LGM (Valdez et al., 2005). However, as already discussed, with the chemistry findings indicating a weak BVOC-OH dependence, the impact of OH increase due to BVOC is not considered for our LGM methane simulation. Since, reduced BVOC itself accounts for 26 % OH rise as shown in Fig. 1, by omitting it from the net OH change, we assume that there was effectively no change in OH between PI and LGM.

ACPD
14, 3193–3230, 2014

4 Results and discussion

4.1 Wetland emissions for the present-day

From our parameterization, the PD global potential wetland area is calculated to be 10.2 km × 10^6 km^2 which lies in the higher range of presently available wetland databases (Lehner et al., 2004; Kaplan, 2002; Aslemann et al., 1989). Our estimate is 10 % higher compared to the Global Lake and Wetland Database (GLWD; Lehner and Döll, 2004), which used the most detailed approach and is therefore taken as a reference for our study. Our parameterization reproduces the GLWD distribution of wetlands well in North and South America, Asia and Africa, but generates somewhat larger areas for Europe and smaller areas for Alaska, respectively (Fig. 2). The global wetland methane emissions are calculated as 132 Tg. Northern mid latitudes (30–60° N) and tropics contribute 71 Tg and 61 Tg, respectively.

We also analyzed the seasonal pattern of wetlands which has been largely ignored in previous studies. Figure 3 shows that vast regions over North America and Canada remain inundated for four to seven months of the year while for some wetlands over Western Europe and Central America the inundation occurs for eight to nine months. Some permanent wetlands, though very small in area, are found in Central Africa and South America close to the equator and near 30° N at the East American coast.

The seasonality of methane emissions is driven by the seasonality of the wetland inundation and the seasonality in soil temperature. During boreal winter (October through April), emissions from the northern wetlands (30–60° N) remain below 5 Tg per month. Emissions increase strongly after April and reach the maximum strength in the month of July with monthly emissions close to 25 Tg per month. As Fig. 4 shows, over northern wetlands, seasonal variability of soil temperature has a major effect on methane flux seasonality. In contrast, methane emissions from tropical wetlands exhibit little seasonality and show a variation of the monthly mean fluxes between 4.5 and 7.2 Tg per month (Fig. 5).

ACPD
14, 3193–3230, 2014

4.2 Present-day atmospheric methane concentrations

The global mean surface PD methane mixing ratio at the lowest model level (0–50 m) is found $1790 \pm 10.8\,\mathrm{nmol\,mol^{-1}}$ from model simulation. In Fig. 6, one can see the regional distribution of surface methane with the hotspots being located over Indian sub-continent, eastern China and largely over central Europe. The mean surface methane mixing ratio agrees well with observations described by Dlugokencky et al. (1994), who report on weekly data across globally distributed network sites measured between 1986 and 2003. The inter-hemispheric methane gradient is calculated as $145 \pm 2.8\,\mathrm{nmol\,mol^{-1}}$ which is consistent with the findings of Dlugokencky et al. (2011).

The comparison between the observed methane mixing ratio at different WDCGG stations with the model data as given in Fig. 7 shows that our model is able to capture the salient features in the observed seasonal cycle reasonably well across the stations. However for few stations situated above 60° north, the seasonality is not too well captured and the model overestimates methane by 20 to $40\,\mathrm{nmol\,mol^{-1}}$. Over the majority of the stations in the tropics and at all of the stations in the Southern Hemisphere, the model is able to reproduce the expected seasonality very well. Here the average model bias is -5 to $-10\,\mathrm{nmol\,mol^{-1}}$, i.e. less than 0.6 %.

It is evident from Fig. 7 that over a number of northern mid-latitude stations situated near the high emission regions, like Black Sea (44.17° N, 28.67° E), Sary Taukum (44.45° N, 75.57° E) and Ulaan Uul (44.45° N, 111.08° E) the model performance is fairly good, although it fails to predict the annual maxima. Over the background sites, e.g. Tudor Hill (32.27° N, 64.87° W), St. Davids Head (32.37° N, 64.65° W) and Terceira Island (38.77° N, 27.37° W), the simulated seasonal cycle agrees very well with the observations. The average correlations between model and observation for the Southern Hemispheric stations are always high with a mean value of 0.98 while they are 0.90 for the tropical stations and 0.77 for the stations between 15 and 30° N. For the northern extra tropical stations the correlation coefficient decreases to 0.61. The

ACPD
14, 3193–3230, 2014

worst correlation (r = 0.3) is found for Hegyhatsal (46.95° N 16.63° W) and Mace Head (53.32° N, 9.90° W). For three stations (Plateau Assy 43.25° N, 77.87° E, Black Sea 44.17° N 28.67° W, Ulaan Uul 44.45° N, 111.08° E) the model seasonality is found to be in the opposite phase to the observations. We speculate that the large discrepancy found at some stations may be due to the omission of local sources in our inventory. Further in north, the correlation improves, and the mean correlation coefficient is 0.8. As the seasonal cycle in this region is dominated by wetland emissions this indicates that the wetland parameterization of our model is adequate.

The average rms error in the southern latitudinal belt, where the model performs best, is 4.2 nmol mol^{-1}. Over the tropical region the rms error increases to 13 nmol mol^{-1} and further north to 20 nmol mol^{-1}. Overall the global average rms is 13 nmol mol^{-1} which, compared to other forward modeling studies, constitutes an excellent agreement. For example, Patra et al. (2009) computed a mean rms error of 18.6 ± 4.2 ppb for the stations situated between the latitudes 5 and 60° N.

Figure 8 shows the latitudinal gradient of observed and simulated methane during one month of each season. Over the Southern Hemisphere, the average methane mixing ratio does not show any significant spatial variability and remains between 1700 and 1750 nmol mol^{-1} during the entire year. Nothward of 5° S (January) or 10° N (August), the methane mixing ratio rises till it reaches a maximum between 1850 and 1900 nmol mol^{-1} at 50 to 60° N. The spread of values among stations in the same latitude band is largest between 20 and 60° N, and we note that the observations show more scatter than the model.

4.3 PI and LGM wetland emissions

During PI, the same CARAIB soil moisture map is used as in the PD run to map potential wetlands since there is no evidence suggesting any significant changes in natural wetlands. Due to the slightly lower soil temperatures in wetland areas, the PI wetland methane emissions are calculated as 115 Tg yr^{-1}, which is 17 Tg lower than its PD value.

ACPD
14, 3193–3230, 2014

For LGM, CARAIB provides soil moisture map from its LGM simulation, which is used for mapping the LGM wetlands in this study, based on the same parameterization approach, as of present day. However, due to the competing factors of ice-covered potential wetland areas in the boreal zone and exposure of additional continental shelves the total wetland area for LGM is estimated to be 7.75×10^6 km^2 of which continental shelves contribute almost 30 %. This wetland area is similar to Webber et al. (2010) but a bit larger than Kaplan et al. (2006) and Valdes et al. (2005). In contrast to the present-day map, the northern latitudes show a reduction of more than 50 %. According to our model, tropical wetlands were almost 15 % larger which is attributed to the coastal shelves especially in Southeast Asia. In spite of the relatively large wetland areas compared to previous studies (Valdes et al., 2005; Kaplan et al., 2006), the Gedney et al. (2004) parameterization yields only 72 Tg yr^{-1} which falls in the low range of the existing inventories and can be explained by our choice of the K_{CH_4} value which was derived for present-day conditions (see Sect. 2.1).

4.4 PI and LGM methane concentrations

The PI methane simulation with the present day OH yields an average surface methane mixing ratio of 745 ± 6 nmol mol^{-1} which is 40 nmol mol^{-1} higher than ice core records (Etheridge et al., 1998; Loulergue et al., 2008). With a 6 % lower than present OH, the model simulates an even higher PI methane, almost by 95 ppb compared to the observation. It indicates that the strength of PI methane sources has to be reduced in order to match with observations. Given the small contribution of individual or combined anthropogenic sources for PI methane simulation, it is likely that our parameterisation overestimates the PI wetland source. If the other sources are assumed to be correct as listed in Table 1, the annual PI wetland methane budget should be 99 and 88 Tg yr^{-1} for unchanged OH and a 6 % lower than present OH, respectively (compared to the calculated value of 115 Tg yr^{-1} as in Table 1).

The LGM simulation yields an annual average methane mixing ratio of 415 ± 4 nmol mol^{-1}, which is higher than the estimate of 360 and 364 nmol mol^{-1} by

ACPD
14, 3193–3230, 2014

Loulergue et al. (2008) and Dällenbach et al. (2000), respectively. Hotspots of elevated methane mixing ratios are found close to the equator over South America and Africa with average values between 426 and 480 nmol mol^{-1}. The Sunda shelf region near present Malaysia yields methane mixing ratios of more than 450 nmol mol^{-1} resulting from the large wetland emissions from exposed shelves. The LGM inter polar gradient, derived by calculating the difference of mean methane mixing ratios between latitudinal bands surrounding Greenland and Antarctica is 22 ± 4 nmol mol^{-1} in good agreement with the Dällenbach et al. (2000) estimate of 14 ± 4 nmol mol^{-1}.

A sensitivity simulation with OH concentrations increased by 25 % as in previous studies yielded a global annual average methane mixing ratio of 345 ± 8 nmol mol^{-1}, slightly lower than the Dällenbach et al. (2000) estimate. Due to the large uncertainties in the source estimates, both LGM simulations are considered consistent with the ice core record. In order to match the observations to within ± 10 nmol mol^{-1}, the total methane emissions would have to be around 96 Tg and 120 Tg for the base run and the run with increased OH, respectively (compared to 116 Tg in our model set-up; Table 1). If the entire uncertainty were due to wetland emissions, the respective changes would have to be a reduction from 72 Tg yr^{-1} to 52 Tg yr^{-1} or an increase to 76 Tg yr^{-1}.

5 Methane changes from LGM to PI and PD

The model simulations of LGM, PI and PD show that the model with a consistent wetland module captures the changes in methane concentration reasonably well, both from LGM to PI and from PI to PD. If the transition from PI to PD is easily explained by increasing anthropogenic emissions, the change of methane from LGM to present day is more complex. The rise in industrial methane emission between PI and PD is 64 % whereas the emission from biomass burning and rice agriculture grew by 75 % and 70 % respectively, according to our inventory. On the other hand, the LGM wetland methane source is estimated to have been reduced by 45 % compared to PD which

ACPD
14, 3193–3230, 2014

is a much stronger reduction than assumed in previous modeling studies. Overall, the total methane sources in LGM are 75 % lower than during PD.

The LGM inter hemispherical difference is only 10 % and 30 % of its PI and PD values, mainly because of the huge reduction of northern hemispherical wetland methane sources. As discussed in Levine et al. (2011), previous studies (Valdes et al., 2005; Kaplan et al., 2006) attributed only about half of the methane concentration changes between LGM and PI to changes in wetland emissions, whereas Weber et al. (2010) suggest a larger change, consistent also with the results from our wetland emission parameterization.

Compared to the magnitude of change of the methane source strengths between LGM and PD, the alterations of methane sinks, mainly the OH concentration are insignificant. The weak BVOC-OH dependence in LGM as indicated from the recent chemistry studies supports this. Though the exact quantification of both the PI and LGM OH deviation would demand a full chemistry study including an OH recycling mechanism, the increase in LGM OH concentration should be marginal. Similarly, a higher than present PI OH (up to 20 %) as found in other studies, seems unrealistic and this study supports the assumption of a PI OH that was similar to present day. Our results indicate that wetlands played a larger role in the LGM to PD transition of the global CH_4 budget than suggested by previous studies. Without any changes in the OH distribution LGM wetland emissions are estimated at 52 $Tg\,yr^{-1}$ which is 60 % less than during PD, while PI wetland emissions should be 25 % less.

6 Conclusions

In this study we used the ECHAM5-MOZ chemistry general circulation model with a new wetland methane emission parameterization in order to consistently simulate the global methane budget for Last Glacial Maximum, pre-industrial, and present-day climate conditions. The new wetland scheme is based on input data on finer spatial resolution of 10 min for present day and pre-industrial and 30 min for LGM. This allows

ACPD
14, 3193–3230, 2014

for a better representation of the regional distribution of wetlands compared to most previous studies and makes it possible to begin evaluating the seasonal cycle of the wetland source.

The model simulations use a consistent set-up for all three climatic periods and reproduce observed methane concentrations from the global station network particularly well for the present day (within the error margin of 2 %). Ice core data for PI and LGM are lower than our simulations by up to 6 and 15 % respectively. These results lend some credibility to the changes in wetland emissions that are produced by our parameterization and also provide useful insight on the dominant role of wetlands in methane changes from LGM to present. It must be noted that our wetland emission parameterization yields lower global annual totals compared to other methane inventories. For present day the annual wetland methane emissions average to 132 ± 10 Tg which is below the range cited in the IPCC AR4 report, while for PI and LGM they are calculated as 116 Tg and 72 Tg, respectively, which is also significantly lower compared to Kaplan et al. (2006), Valdes et al. (2005), and Weber et al. (2010). According to our simulations, the LGM wetland methane emissions were 45 % lower than during PD. This reduction is much stronger than the changes estimated by Kaplan (2002) and Valdes et al. (2005), which found a reduction by 25 % and 27 %, respectively. Weber et al. (2010) found comparable changes between 35 and 42 %.

Our low LGM wetland emissions are supported by recent findings of a much stronger chemical buffering of the OH concentration in environments with high biogenic VOC concentrations (Hofzumahaus et al., 2009; Lu et al., 2012). While there is an ongoing discussion about the exact nature of the chemical pathways which recycle OH under conditions of low NO_x and high isoprene (Peeters et al., 2009; Taraborrelli et al., 2012; Archibald et al., 2011), this finding challenges the former hypothesis that substantially reduced BVOC emissions during LGM would lead to much higher OH concentrations, and therefore a reduced methane lifetime. Our model results with the consistent wetland emission parameterisation and no changes in OH yield a reasonable agreement with observations. For a full understanding of the impact of the newly discovered iso-

ACPD
14, 3193–3230, 2014

prene chemistry one would have to know the reaction pathways and rates and run the model with fully interactive chemistry. So far, OH recycling has only been implemented by Levine et al. (2011). In contrast to our assumptions, their results indicated that OH buffering should not have a significant impact on the methane lifetime because it gets cancelled due to equal and opposite effect of changes in air temperature.

In summary, our modeling study suggests that past changes in the methane concentration were primarily driven by changes in the wetland emission source and changes in the methane sink due to OH oxidation were marginal. Thus confirming the conclusion of Levine et al. (2011) of almost entirely source-driven PI-LGM methane transition. Moreover this study also extends this conclusion to the methane changes from the pre-industrial to the present-day era. While Levine et al. (2011) had focused their study on the sensitivity of methane concentrations and lifetimes to atmospheric chemistry processes, our simulations include the explicit calculation of changes in wetland emissions and climate. A logical next step would be fully interactive climate-chemistry simulations to understand feedbacks involved.

The service charges for this open access publication
have been covered by a Research Centre of the
Helmholtz Association.

References

Adams, J. M., Constable, J. V. H., Guenther, A. B., and Zimmerman, P.: An estimate of natural volatile organic compound emissions from vegetation since the Last Glacial Maximum, Chemosphere, 3, 73–91, 2001.

Archibald, A. T., Levine, J. G., Abraham, N. L., Cooke, M. C., Edwards, P. M., Heard, D. E., Jenkin, M. E., Karunaharan, A., Pike, R. C., Monks, P. S., Shallcross, D. E., Telford, P. J., Whalley, L. K., and Pyle, J. A.: Impacts of HO_x regeneration and recycling in the oxidation of isoprene: consequences for the composition of past, present and future atmospheres, Geophys. Res. Lett., 38, L05804, doi:10.1029/2010GL046520, 2011.

ACPD
14, 3193–3230, 2014

Aselmann, I. and Crutzen, P. J.: Global distribution of natural freshwater wetlands and rice paddies, their net primary productivity, seasonality and possible methane emissions, J. Atmos. Chem., 8, 307–358, 1989.
Asselin, R.: Frequency filter for time integrations, Am. Meteorol. Soc., 100, 487–490 1972.
Blunier, T., Chappellaz, J., Schwander, J., Stauffer, B., and Raynaud, D.: Variations in atmospheric methane concentration during the Holocene epoch, Nature, 374, 46–49, 1995.
Bubier, J. L., Moore, T. R., and Roulet, N. T.: Methane emissions from mid-boreal wetlands of northern Ontario, Canada, Ecology, 74, 2240–2254, 1993.
Cao, M., Marshall, S., and Gregson, K.: Global carbon exchange and methane emissions from natural wetlands: application of a process-based model, J. Geophys. Res., 101, 14399–14414, 1996.
Chang, T.: The origin, evolution, cultivation, dissemination, and diversification of Asian and African rices, Euphytica, 25, 425–441, 1976.
Chappellaz, J. A. and Fung, I. Y.: The atmospheric CH_4 increase since the Last Glacial Maximum (1). Source estimates, Tellus B, 45, 228–241, 1993.
Chappellaz, J., Barnola, J. M., Raynaud, D., Korotkevich, Y. S., and Lorius, C.: Ice-core record of atmospheric methane over the past 160,000 years, Nature, 345, 127–131, doi:10.1038/345127a0, 1990.
Chappellaz, J., Bluiner, T., Kints, S., Dällenbach, A., Barnola, J.-M., Schwander, J., Raynaud, D., and Stauffer, B.: Changes in the atmospheric CH_4 gradient between Greenland and Antarctica during the Holocene, J. Geophys. Res., 102, 15987–15997, 1997.
Crutzen, P. J. and Brühl, C.: A model study of atmospheric temperatures and the concentration of ozone, hydroxyl and some other photochemical active gases during the glacial, the preindustrial Holocene and the present, Geophys. Res. Lett., 20, 1047–1050, 1993.
Cunnold, D. M., Steele, L. P., Fraser, P. J., Simmonds, P. G., Prinn, R. G., Weiss, R. F., Porter, L. W., O'Doherty, S., Langenfelds, R. L., Krummel, P. B., Wang, H. J., Emmons, L., Tie, X. X., and Dlugokencky, E. J.: In situ measurements of atmospheric methane at GAGE/AGAGE sites during 1985–2000 and resulting source inferences, J. Geophys. Res., 107, D14225, doi:10.1029/2001JD001226, 2002.
Dällenbach, A., Blunier, T., Flückiger, J., Stauffer, B., Chappellaz, J., and Raynaud, D.: Changes in the atmospheric CH_4 gradient between Greenland and Antarctica during the Last Glacial and the transition to the Holocene, Geophys. Res. Lett., 27, 1005–1008, 2000.

ACPD
14, 3193–3230, 2014

Dlugokencky, E. J., Steele, L. P., Lang, P. M., and Masarie, K. A.: The growth rate and distribution of atmospheric methane, J. Geophys. Res., 99, 17021–17043, 1994.
Dlugokencky, E. J., Steele, L. P., Lang, P. M., and Masarie, K. A: Atmospheric methane at Mauna Loa and Barrow observatories: presentation and analysis of in situ measurements, J. Goephys. Res., 100, 23103–23113, 1995.
Dlugokencky, E. J., Masarie, K. A., Lang, P. M., and Tans, P. P.: Continuing decline in the growth rate of the atmospheric methane burden, Nature, 393, 447–450, 1998.
Dlugokencky, E. J., Nisbet, E. G., Fischer, R., and Lowry, D.: Global atmospheric methane: budget, changes and dangers, Philos. T. R. Soc., 369, 2058–2072, 2011.
Dowsett, H., Foley, K., Stoll, D., Chandler, M., Sohl, L., Bentsen, M., Otto-Bliesener, B., Bragg, F., Chan, W., Contoux, C., Dolan, A., Haywood, A., Jonas, J., Jost, A., Kamae, Y., Lohmann, G., Lunt, D., Nisancioglu, K., Abe-Ouchi, A., Ramstein, G., Riseeslman, C., Robinson, M., Rosenbloom, N., Salzmann, U., Stepanek, C., Strother, S., Ueda, H., Han, Q., and Zhang, Z.: Sea surface temperature of the mid-Piacenzian Ocean: a data–model comparison, Sci. Rep., 3, 189–198, 2013.
Dury, M., Hambuckers, A., Warnant, P., Henrot, A., Favre, E., Ouberdous, M., François, L.: Responses of European forest ecosystems to 21st century climate: assessing changes in interannual variability and fire intensity, iForest – Biogeosciences and Forestry, 4, 82–89, 2011.
Etheridge, D., Steele, L., Francey, R., and Langenfelds, R.: Atmospheric methane between 1000 A. D., and present: evidence of anthropogenic emissions and climate variability, J. Geophys. Res., 103, 15979–15993, 1998.
Etiope, G.: Natural emissions of methane from geological seepage in Europe, Atmos. Environ., 43, 1430–1443, 2009.
Gates, W. L., Boyle, J. S., Covey, C., Dease, C. G., Doutriaux, C. M., Drach, R. S., Fiorino, M., Gleckler, P. J., Hnilo, J. J., Marlais, S. M., Phillips, T. J., Plotter, G. L., Santer, B. J., Sperber, K. R., Taylor, K. E., and Williams, D. N.: An overview of the results of the Atmospheric Model Intercomparison Project (AMIP I), B. Am. Meteorol. Soc., 80, 29–55, doi:10.1175/1520–0477(1999)080<0029:AOOTRO>2.0.CO;2, 1999.
Gedney, N., Cox, P. M., and Huntingford, C.: Climate feedback from wetland methane emissions, Geophys. Res. Lett., 31, L20503, doi:10.1029/2004GL020919, 2004.
Gérard J. C., Nemry, B., François, L., and Warnant, P.: The interannual change of atmospheric CO_2: contribution of subtropical ecosystems?, Geophys. Res. Lett., 26, 243–246, 1999.

ACPD
14, 3193–3230, 2014

Glover, I. C. and Higham, C.: New evidence for early rice cultivation in South, Southeast and East Asia, in: The Origins and Spread of Agriculture and Pastorlaism in Eurasia, edited by: Haris, D. R., UCL Press, London, 413–441, 1996.

Gong, X., Knorr, G., Lohmann, G., and Zhang, X.: Dependence of abrupt Atlantic meriodional ocean circulation changes on climate background states, Geophys. Res. Lett., 40, 3698–3704, 2013.

Gupta, A. K.: In origin of agriculture and domestication of plants and animals linked to early Holocene climate amelioration, Curr. Sci. India, 87, 54–59, 2004.

Henrot, A.-J., François, L., Brewer, S., and Munhoven, G.: Impacts of land surface properties and atmospheric CO_2 on the Last Glacial Maximum climate: a factor separation analysis, Clim. Past, 5, 183–202, doi:10.5194/cp-5-183-2009, 2009.

Hofzumahaus, A., Rohrer, F., Lu, K., Bohn, B., Brauers, T., Chang, C., Fuchs, H., Holland, F., Mita, K., Kondo, Y., Li, X., Lou, S., Shao, M., Zhang, L., Wahner, A., and Zhang, Y.: Amplified trace gas removal in the Troposphere, Science, 324, 1702, doi:10.1126/science.1164566, 2009.

Horowitz, L. W., Walters, S., Mauzerall, D. L., Emmons, L. K., Rasch, P. J., Granier, C., Tie, X., Lamarque, J.-F., Schultz, M. G., Tyndall, G. S., Orlando, J. J., and Brasseur, G. P.: A global simulation of tropospheric ozone and related tracers: description and evaluation of MOZART, version 2, J. Geophys. Res., 108, D24784, doi:10.1029/2002JD002853, 2003.

Houweling, S., Dentener, F., and Lelieveld, J.: Simulation of preindustrial atmospheric methane to constrain the global source strength of natural wetlands, J. Geophys. Res., 105, 17243–17255, 2000a.

Houweling, S., Dentener, F., Lelieveld, J., Walter, B., and Dlugokencky, E.: The modeling of tropospheric methane: how well can point measurements be reproduced by a global model?, J. Geophys. Res., 105, 8981–9002, 2000b.

Jungclaus, J. H., Lorenz, S. J., Timmreck, C., Reick, C. H., Brovkin, V., Six, K., Segschneider, J., Giorgetta, M. A., Crowley, T. J., Pongratz, J., Krivova, N. A., Vieira, L. E., Solanki, S. K., Klocke, D., Botzet, M., Esch, M., Gayler, V., Haak, H., Raddatz, T. J., Roeckner, E., Schnur, R., Widmann, H., Claussen, M., Stevens, B., and Marotzke, J.: Climate and carbon-cycle variability over the last millennium, Clim. Past, 6, 723–737, doi:10.5194/cp-6-723-2010, 2010.

Kageyama, M., Merkel, U., Otto-Bliesner, B., Prange, M., Abe-Ouchi, A., Lohmann, G., Ohgaito, R., Roche, D. M., Singarayer, J., Swingedouw, D., and Zhang, X.: Climatic impacts

ACPD
14, 3193–3230, 2014

of fresh water hosing under Last Glacial Maximum conditions: a multi-model study, Clim. Past, 9, 935–953, doi:10.5194/cp-9-935-2013, 2013.
Kaplan, J. O.: Wetlands at the Last Glacial Maximum: distribution and methane emissions, Geophys. Res. Lett., 29, 1079–1082, 2002.
Kaplan, J. O., Folberth, G., and Hauglustaine, D. A.: Role of methane and biogenic volatile organic compound sources in last glacial and Holocene fluctuations of atmospheric methane concentrations, Global Biogeochem. Cy., 20, GB2016, doi:10.1029/2005GB002590, 2006.
Khalil, M. A. and Ramussen, R. A.: The changing composition of Earth's atmosphere, in: Composition, Chemistry, and Climate of the Atmosphere, edited by: Singh, H. B., Van Nostrand Reinhold, Hoboken, NJ, 50–87, 1995.
Knorr, G., Butzin, M., Micheels, A., and Lohmann, G.: A warm Miocene climate at low atmospheric CO_2 levels, Geophys. Res. Lett., 38, 1–5, 2011.
Krol, M. and Leliveld, J.: Can the variability in tropospheric OH be deduced from measurements of 1,1,1-trichloroethane (methylchloroform)?, J. Geophys. Res., 108, 10697–10711, 2003.
Laurent, J. M., François, L., Bar-Hen, A., Bel, L., and Cheddadi, R.: European bioclimatic affnity groups: data model comparisons, Global Planet. Change, 61, 28–40, 2008.
Lehner, B. and Döll, P.: Development and validation of a global database of lakes, reservoirs and wetlands, J. Hydrol., 296, 1–22, 2004.
Lelieveld, J., Crutzen, P. J., and Dentener, F. J.: Changing concentration, lifetime and climate forcing of atmospheric methane, Tellus B, 50, 128–150, 1998.
Lelieveld. J., Butler, T. M., Crowley, J. N., Dillon, T. J., Fischer, H., Ganzeveld, L., Harder, H., Lawrence, M. G., Martinez, M., Taraborrelli, D., and Williams, J.: Atmospheric oxidation capacity sustained by a tropical forest, Nature, 452, 737–740, 2008.
Levine, J. G., Wolff, E. W., Jones, A. E., Sime, L. C., Valdes, P. J., Archibald, A. T., Carver, G. D., Warwick, N. J., and Pyle, J. A.: Reconciling the changes in atmospheric methane sources and sinks between the Last Glacial Maximum and the pre-industrial era, Geophys. Res. Lett., 38, L23804, doi:10.1029/2011GL049545, 2011.
Li, C., Qui, J., Frolking, S., Xiao, X., Salas, W., Moore III, B., Boles, S., Huang, Y., and Sass, R.: Reduced methane emissions from large scale changes in water management in China's rice paddies during 1980–2000, Geophys. Res. Lett., 30, 1414, doi:10.1029/2002GL015370, 2002.

ACPD
14, 3193–3230, 2014

Loulergue, L., Schilt, A., Spahni, R., Masson-Delmotte, V., Bluiner, T., Lemieux, B., Barnola, J., Raynaud, D., Stocker, T., and Chappellaz, J.: Orbital and millennial-scale feature of atmospheric CH_4 over the past 800,000 years, Nature, 453, 383–386, 2008.

Lu, K. D., Rohrer, F., Holland, F., Fuchs, H., Bohn, B., Brauers, T., Chang, C. C., Häseler, R., Hu, M., Kita, K., Kondo, Y., Li, X., Lou, S. R., Nehr, S., Shao, M., Zeng, L. M., Wahner, A., Zhang, Y. H., and Hofzumahaus, A.: Observation and modelling of OH and HO_2 concentrations in the Pearl River Delta 2006: a missing OH source in a VOC rich atmosphere, Atmos. Chem. Phys., 12, 1541–1569, doi:10.5194/acp-12-1541-2012, 2012.

Martinerie, P., Brasseur, G. P., and Granier, C.: The chemical composition of ancient atmospheres: a model study constrained by ice core data, J. Geophys. Res., 100, 14291–14304, 1995.

Matthews, E., Fung, I., and Lerner, J.: Methane emission from rice cultivation: geographic and seasonal distribution of cultivated areas and emissions, Global Biogeochem. Cy., 5, 3–24, 1991.

Montzka, S. A., Krol, M., Dlugokencky, E., Hall, B., Jöckel, P., and Lelieveld, J.: Small interannual variability of global atmospheric hydroxyl, Science, 331, 67–69, 2011.

Morimoto, S., Aoki, S., Nakazawa, T., and Yamanouchi, T.: Temporal variations of the carbon isotope ratio of atmospheric methane observed at Ny Ålesund, Svalbard from 1996 to 2004, Geophys. Res. Lett., 33, L01807, doi:10.1029/2005GL024648, 2006.

Naik, V., Voulgarakis, A., Fiore, A. M., Horowitz, L. W., Lamarque, J.-F., Lin, M., Prather, M. J., Young, P. J., Bergmann, D., Cameron-Smith, P. J., Cionni, I., Collins, W. J., Dalsøren, S. B., Doherty, R., Eyring, V., Faluvegi, G., Folberth, G. A., Josse, B., Lee, Y. H., MacKenzie, I. A., Nagashima, T., van Noije, T. P. C., Plummer, D. A., Righi, M., Rumbold, S. T., Skeie, R., Shindell, D. T., Stevenson, D. S., Strode, S., Sudo, K., Szopa, S., and Zeng, G.: Preindustrial to present-day changes in tropospheric hydroxyl radical and methane lifetime from the Atmospheric Chemistry and Climate Model Intercomparison Project (ACCMIP), Atmos. Chem. Phys., 13, 5277–5298, doi:10.5194/acp-13-5277-2013, 2013.

Otto, D., Rasse, D., Kaplan, J., Warnant, P., and François, L.: Biospheric carbon stocks reconstructed at the Last Glacial Maximum: comparison between general circulation models using prescribed and sea surface temperatures, Global Planet. Change, 33, 117–138, 2002.

Peeters, J. and Müller, J.: HO_x radical regeneration in isoprene oxidation via peroxy radical isomerisms. II: experimental evidence and global impact, Phys. Chem. Chem. Phys., 12, 14227–14235, 2010.

ACPD
14, 3193–3230, 2014

Peeters, J., Nquyen, T. L., and Vereecken, L.: HO_x radical regeneration in the oxidation of isoprene, Phys. Chem. Chem. Phys., 11, 5935–5939, 2009.
Prinn, R. G., Huang, J., Weiss, R. F., Cunnold, D. M., Fraser, P. J., Simmonds, P. G., McCulloch, A., Harth, C., Reimann, S., Salameh, P., O'Doherty, S., Wang, R. H. J., Porter, L. W., and Miller, B. R.: Evidence for substantial variations of atmospheric hydroxyl radicals in the past two decades, Science, 292, 1882–1888, 2001.
Quay, P. J., King, S. L., White, D., Brockington, M., Plotkin, B., Gammon, R., Gerst, S., and Stutsman, J.: Atmospheric ^{14}CO: a tracer of OH concentration and mixing rates, J. Geophys. Res., 105, 15147–15166, 2000.
Robert, A. J.: A semi-Lagrangian and semi-implicit numerical integration scheme for the primitive meteorological equations, J. Meteorol. Soc. Jpn., 60, 319–325, 1982.
Roeckner, E., Bäuml, G., Bonaventura, L., Brokopf, R., Esch, M., Giorgetta, M., Hagemann, S., Kirchner, I., Kornblueh, L., Manzini, E., Rhodin, A., Schlese, U., Schulzweida, U., and Tompkins, A.: The atmospheric general circulation model ECHAM5, part I: Model description, Report No. 349, Max Planck Institute for Meteorology, 2003.
Ruddiman, W. F. and Thomson, J. S.: The case for human cause of increased atmospheric CH_4 over the last 5000 years, Quaternary Sci. Rev., 20, 1769–1777, 2001.
Sander, S., Friedl, R., Barkern, J., Golden, D., Kurylo, M., Wine, P., Abbat, J., Moortgaret, C., Huie, R., and Orkin, R. E.: Chemical Kinetics and Photochemical Data for Use in Atmospheric Studies, Technical Report, NASA/JPL Publication 17, 27822, 27823, 27826, 27830, 2011.
Schultz, M. G., Heil, A., Hoelzemann, J. J., Spessa, A., Thonicke, K., Hoelzemann, J., Spessa, A., Goldammer, J. G., Held, A. C., Pereira, J. M. C., and van het Bolscher, M.: Global wildland fire emissions from 1960 to 2000, Global Biogeochem. Cy., 22, GB2002, doi:10.1029/2007GB003031, 2008.
Shindell, D. T., Grenfell, J., Rind, D., and Grewel, V.: Chemistry-climate interactions in the Goddard Institute for Space Studies general circulation model 1. Tropospheric chemistry model description and evaluation, J. Geophys. Res., 106, 8047–8075, 2001.
Simmons, A. J. and Burridge, D. M.: An energy and angular momentum conserving vertical finite difference scheme and hybrid vertical coordinates, Mon. Weather Rev., 109, 758–766, 1981.
Spahni, R., Chappellaz, J., Stocker, T. F., Loulergue, L., Hausammann, G., Kawamura, K., Flückiger, J., Schwander, J., Raynaud, D., Masson-Delmotte, V., and Jouzel, J.: Atmospheric

ACPD
14, 3193–3230, 2014

methane and nitrous oxide of the late Pleistocene from Antarctic ice cores, Science, 310, 1317, doi:10.1126/science.1120132, 2005.
Stauffer, B., Lochboronner, E., Oeschger, H., and Schwander, J.: Methane concentration in the glacial atmosphere was only half of the preindustrial Holocene, Nature, 332, 812–814, 1988.
Stepanek, C. and Lohmann, G.: Modelling mid-Pliocene climate with COSMOS, Geosci. Model Dev., 5, 1221–1243, doi:10.5194/gmd-5-1221-2012, 2012.
Stevenson, D. S., Dentener, F. J., Schultz, M. G., Ellingsen, K., van Noije, T. P. C., Wild, O., Zeng, G., Amann, M., Atherton, C. S., Bell, N., Bergmann, D. J., Bey, I., Butler, T., Cofala, J., Collins, W. J., Derwent, R. G., Doherty, R. M., Drevet, J., Eskes, H. J., Fiore, A. M., Gauss, M., Hauglustaine, D. A., Horowitz, L. W., Isaksen, I. S. A., Krol, M. C., Lamarque, J.-F., Lawrence, M. G., Montanaro, V., Müller, J.-F., Pitari, G., Prather, M. J., Pyle, J. A., Rast, S., Rodriguez, J. M., Sanderson, M. G., Savage, N. H., Shindell, D. T., Strahan, S. E., Sudo, K., and Szopa, S.: Multi-model ensemble simulations of present-day and near-future tropospheric ozone, J. Geophys. Res., 111, D08301, doi:10.1029/2005JD006338, 2006.
Subak, S.: Methane from the House of Tudor and the Ming Dynasty, Chemosphere, 29, 843–854, 1994.
Sueyoshi, T., Ohgaito, R., Yamamoto, A., Chikamoto, M. O., Hajima, T., Okajima, H., Yoshimori, M., Abe, M., O'ishi, R., Saito, F., Watanabe, S., Kawamiya, M., and Abe-Ouchi, A.: Set-up of the PMIP3 paleoclimate experiments conducted using an Earth system model, MIROC-ESM, Geosci. Model Dev., 6, 819–836, doi:10.5194/gmd-6-819-2013, 2013.
Taraborrelli, D., Lawrence, M. G., Crowley, J. N., Dillon, T. J., Gromov, S., Groß, C. B. M., Vereecken, L., and Leileveld, J.: Hydroxyl radical buffered by isoprene oxidation over tropical forest, Nat. Geosci., 5, 190–193, 2012.
Thompson, A. M., Chappellaz, J., Fung, I. Y., and Kucsera, T.: The atmospheric CH_4 increase since the Last Glacial Maximum. (2), Interactions with oxidants, Tellus B, 45, 242–257, 1993.
Valdes, P. J., Beerling, D. J., and Johnson, C. E.: The ice age methane budget, Geophys. Res. Lett., 32, L02704, doi:10.1029/2004GL021004, 2005.
Varma, V., Prange, M., Merkel, U., Kleinen, T., Lohmann, G., Pfeiffer, M., Renssen, H., Wagner, A., Wagner, S., and Schulz, M.: Holocene evolution of the Southern Hemisphere westerly winds in transient simulations with global climate models, Clim. Past, 8, 391–402, doi:10.5194/cp-8-391-2012, 2012.
Wang, Y. and Jacob, D.: Anthropogenic forcing on tropospheric ozone and OH since preindustrial times, J. Geophys. Res., 103, 3399–3417, 1998.

ACPD
14, 3193–3230, 2014

Warnant, P., François, L., Strivay, D., and Gérard, J. C.: CARAIB: a global model of terrestrial biological productivity, Global Biogeochem. Cy., 8, 255–270, 1994.
Weber, S. L., Drury, A. J., Toonen, W. H. J., and van Weele, M.: Wetland methane emissions during the Last Glacial Maximum estimated from PMIP2 simulations: climate, vegetation, and geographic controls, J. Geophys. Res., 115, D06111, doi:10.1029/2009JD012110, 2010.
Wei, W. and Lohmann, G.: Simulated Atlantic multidecadal oscillation during the Holocene, J. Climate, 25, 6989–7002, 2012.
Wei, W., Lohmann, G., and Dima, M.: Distinct modes of internal variability in the global meridional overturning circulation associated with the Southern Hemisphere westerly winds, J. Phys. Oceanogr., 42, 785–801, 2012.
Wuebbles, D. J. and Hayhoe, K.: Atmospheric methane and global change, Earth-Sci. Rev., 57, 177–210, 2002.
Zhang, X., Lohmann, G., Knorr, G., and Xu, X.: Different ocean states and transient characteristics in Last Glacial Maximum simulations and implications for deglaciation, Clim. Past, 9, 2319–2333, doi:10.5194/cp-9-2319-2013, 2013.

ACPD
14, 3193–3230, 2014

Table 1. Methane emission strengths in $Tgyr^{-1}$ as used in ECHAM simulation for present day, PI and LGM.

	Emission for present day simulation (in $Tgyr^{-1}$)	Emission for PI simulation (in $Tgyr^{-1}$)	Emission for LGM simulation (in $Tgyr^{-1}$)
Natural			
Wetlands	132	115	72
Termites	19	19	27
Ocean	17	15	10
Hydrates	–	–	–
Geological seepage	–	–	–
Wild animals	8.5	15	–
Anthropogenic			
Energy	83	–	–
Landfills and Waste	76	–	–
Ruminants	101	12	–
Rice (seasonal)	40	10	–
Biomass burning	35	10	7
Total	510	196	116

ACPD
14, 3193–3230, 2014

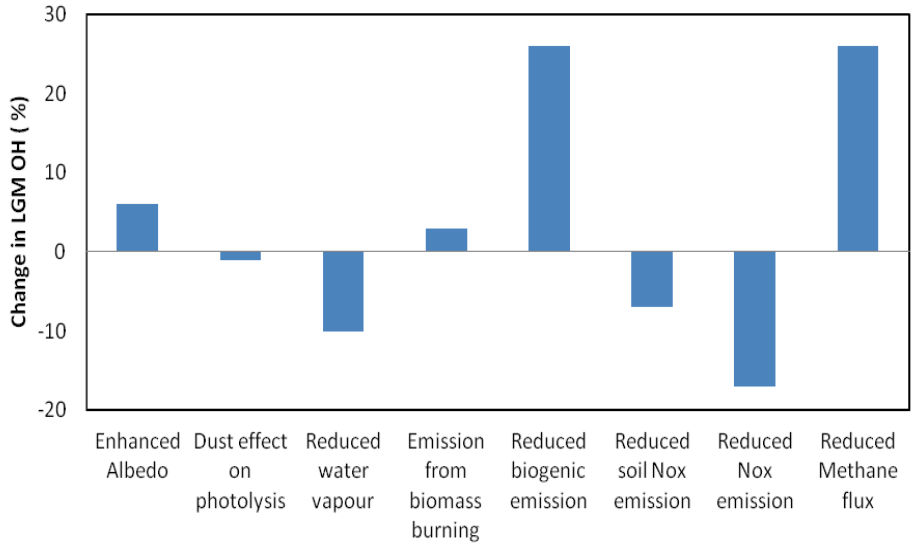

Fig. 1. Effect of various factors on LGM OH change with respect to PI as simulated by MOZART2 chemistry transport model.

ACPD
14, 3193–3230, 2014

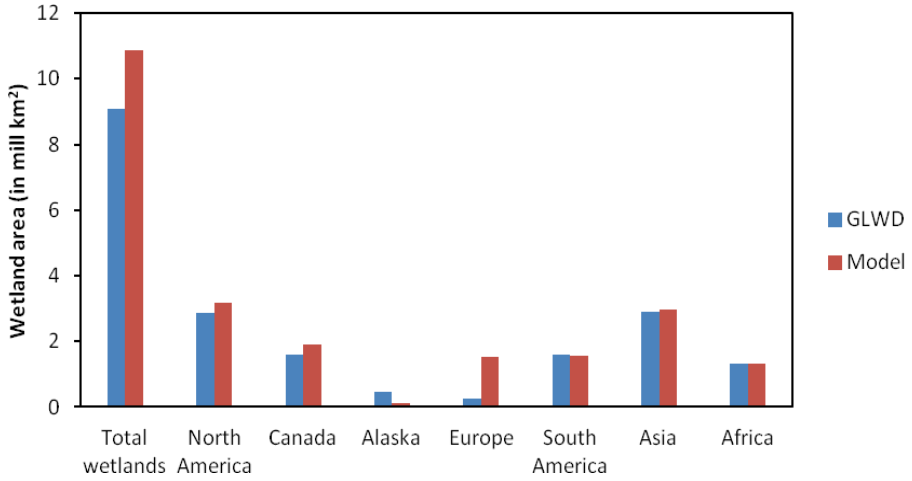

Fig. 2. Regionally aggregated wetland areas from this study compared to the Global Lake and Wetland Database (GLWD) of Lehner and Döll (2004).

ACPD
14, 3193–3230, 2014

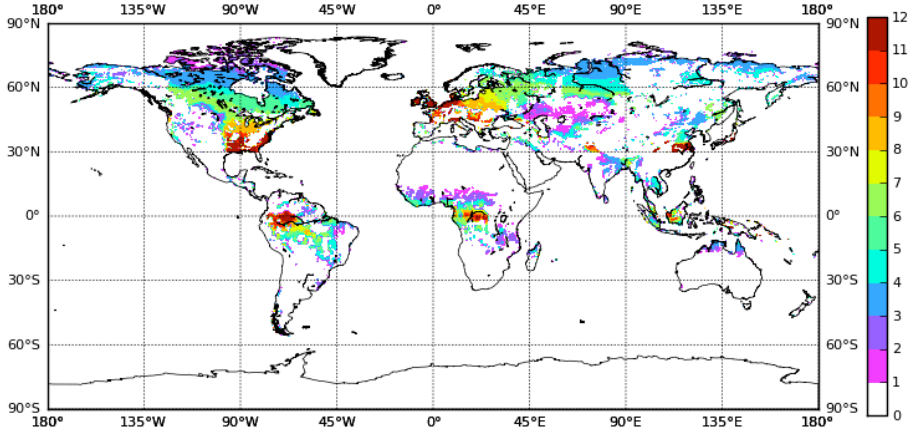

Fig. 3. Duration of wetland inundation in months from this study. The colour bar represents the number of months in a year over which wetlands occur.

ACPD
14, 3193–3230, 2014

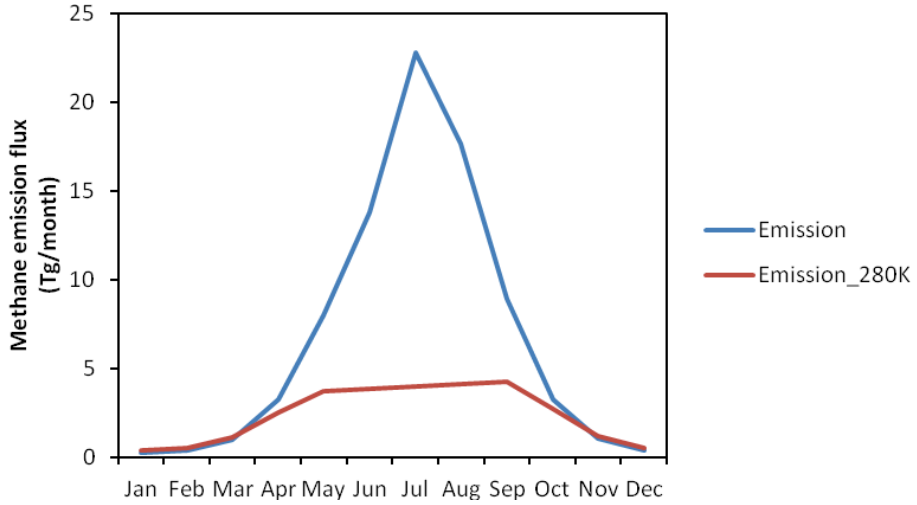

Fig. 4. Impact of soil temperature variability on CH_4 emissions seasonality from wetlands at north of 30° N. The blue curve shows the actual monthly methane emission ($Tg\,month^{-1}$) while the red curve shows the theoretical emission pattern in a scenario where the soil temperature is kept fixed at 280 K throughout the year.

ACPD
14, 3193–3230, 2014

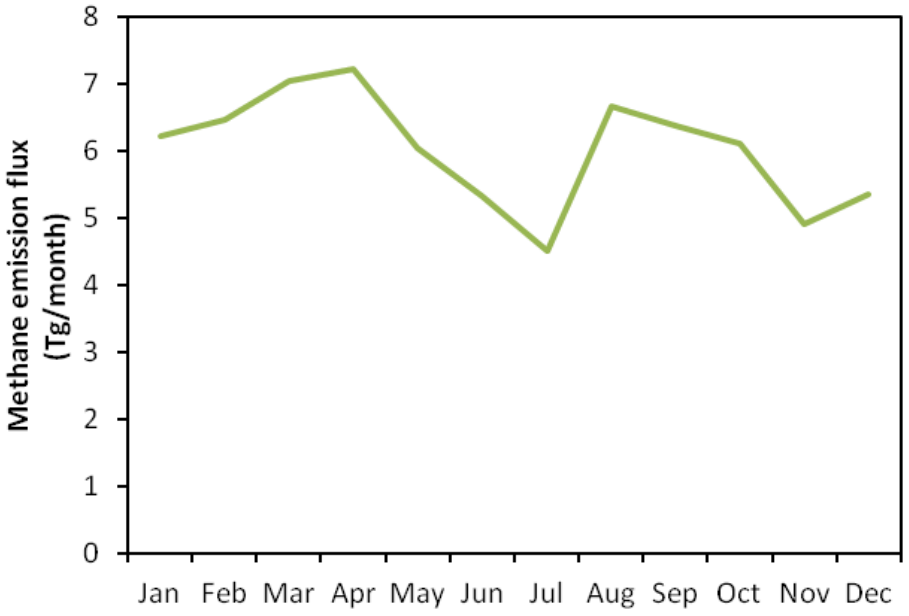

Fig. 5. Seasonal variation of monthly CH_4 emissions (Tg month^{-1}) from tropical wetlands.

ACPD
14, 3193–3230, 2014

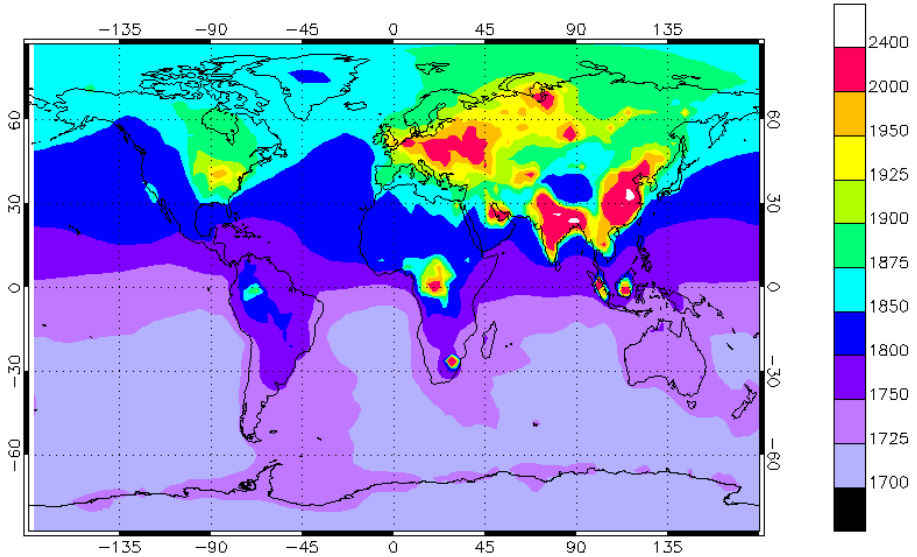

Fig. 6. Annual mean present day surface methane distribution (in nmol mol^{-1}) from the ECHAM5 atmospheric model simulation.

ACPD
14, 3193–3230, 2014

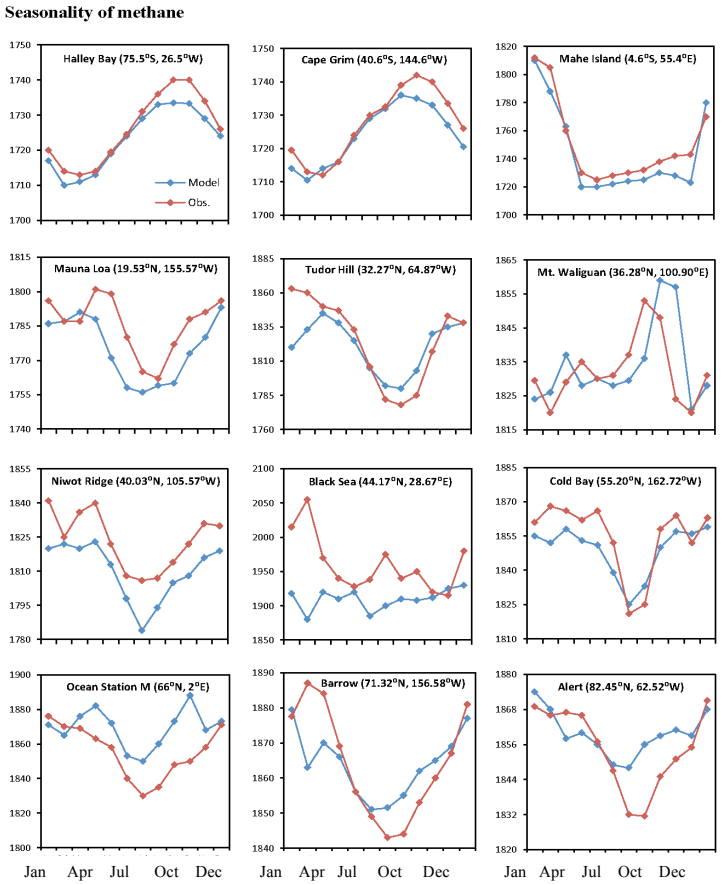

Fig. 7. Model-observation comparison of surface methane mixing ratios (in nmol mol^{-1}) at selected sites. Observations are averaged between 1986 and 2006. The model data is the monthly average of output of four years in its equilibrium state.

ACPD
14, 3193–3230, 2014

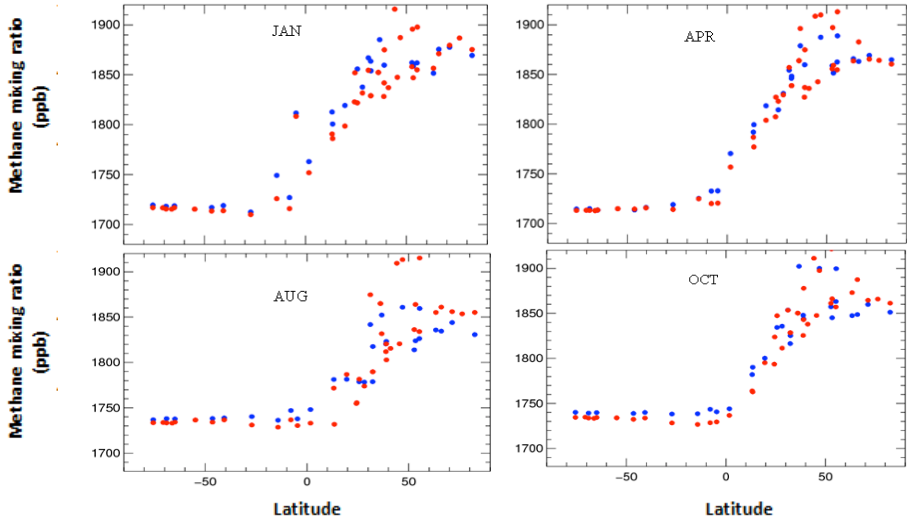

Fig. 8. Comparison between model and observations for the latitudinal distribution of surface methane mixing ratio at different months of the year (January, April, August and October). The red and blue symbols stand for the observation and model respectively.

ACPD
14, 3193–3230, 2014

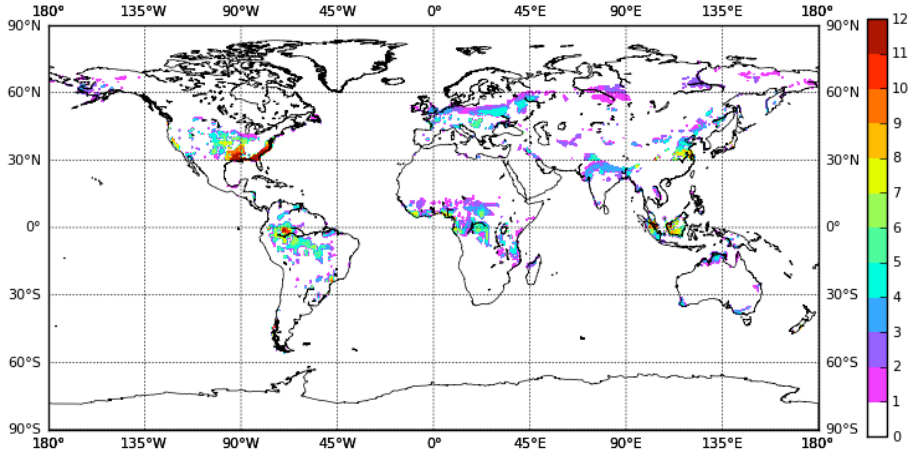

Fig. 9. Distribution of potential LGM wetlands with the color bar indicating monthly frequency of inundation over a climatological year.

ACPD
14, 3193–3230, 2014

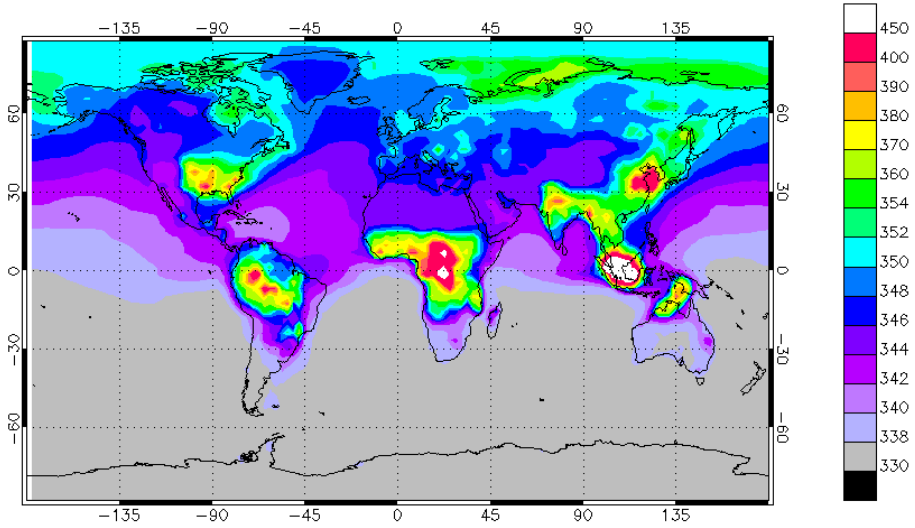

Fig. 10. The spatial distribution of the annual mean surface methane mixing ratio (in nmol mol^{-1}) for LGM from ECHAM5 atmospheric model simulation.

ACPD
14, 3193–3230, 2014